Published in final edited form as:
J Am Soc Echocardiogr. 2007 May ; 20(5): 539–551.

Left Ventricular Form and Function Revisited: Applied Translational Science to Cardiovascular Ultrasound Imaging

Partho P. Sengupta, MBBS, MD, DM, **Vijay K. Krishnamoorthy, MBBS, MD**, **Josef Korinek, MD**, **Jagat Narula, MBBS, MD, DM, PhD, FACC, FAHA**, **Mani A Vannan, MBBS, FACC**, **Steven J Lester, MD, FACC, FRCPC**, **Jamil A. Tajik, MBBS, MD, FACC**, **James B Seward, MD, FACC**, **Bijoy K. Khandheria, MBBS, FACC, FASE, FESC**, and **Marek Belohlavek, MD, PhD, FACC, FESC**

From the Division of Cardiovascular Diseases (P.P.S., V.K.K, J.K., J.B.S.), Mayo Clinic, Rochester, Minnesota; the Division of Cardiology (J.N., M.A.V.), University of California at Irvine, Irvine, California; and the Division of Cardiovascular Diseases (S.J.L., J.A.T., B.K.K., M.B.), Mayo Clinic Arizona, Scottsdale, Arizona

Abstract

Tissue Doppler imaging (TDI) and TDI-derived strain imaging are robust physiologic tools used for the noninvasive assessment of regional myocardial function. Due to high temporal and spatial resolution, regional function can be assessed for each phase of the cardiac cycle and within the transmural layers of the myocardial wall. Newer techniques that measure myocardial motion by speckle tracking in grayscale images have overcome the angle dependence of TDI strain, allowing for measurement of 2-dimensional strain and cardiac rotation. TDI, TDI strain, and speckle tracking may provide unique information that deciphers the deformation sequence of complexly oriented myofibers in the left ventricular wall. The data are, however, limited. This review examines the structure and function of the left ventricle relative to the potential clinical application of TDI and speckle tracking in assessing the global mechanical sequence of the left ventricle in vivo.

The spiral arrangement of muscle fibers in the heart is reminiscent of spiral and vortex patterns in nature, ranging from small organelles and whirlpools to hurricanes and rotational patterns of the galaxies (1–5). Vortex patterns link two fundamental forms of motion that work in close balance: an inner, rapidly descending swirl and an outer, less rapid, ascending rotation (4) (Fig. 1 A–C). These counterdirectional movements of a vortex produce suction and expulsion forces that have been exploited for designing energy efficient propellers and turbines (6). Likewise, experimental and mathematical modeling of the clockwise and counterclockwise spiral loops of myofibers in the left ventricle (LV) has shown that counterdirectional geometry provides an efficient distribution of regional stresses and strains (7). Conversely, altered ventricular geometry resulting from cardiac remodeling, regional myocardial dysfunction, or asynchronous conduction distort the efficiency of the loading and expulsion dynamics (8,9). In this review, we associate the LV myofiber architecture to the spatiotemporal sequence of regional deformations occurring during normal cardiac contraction and relaxation. We further elucidate experimental observations, which explore the application of tissue Doppler imaging (TDI) and 2-dimensional ultrasound speckle tracking for delineation of the synchronous mechanical shortening and lengthening sequences of the human LV.

Address reprint requests to Marek Belohlavek, Division of Cardiovascular Diseases, Mayo Clinic, 13400 East Shea Boulevard Scottsdale, AZ 85259, E-mail address for author named in reprint line: Belohlavek.marek@mayo.edu

Myofiber architecture of the left ventricle

Emergence of spiral myofiber architecture in the LV occurs following several sequential embryonic stages (10). In the early tubular heart, the walls of the LV develop from two layers of epithelial cells. In the later (second) stage, proliferation and growth of the inner layer results into formation of sheets and chords that develop gradually into inner centripetally aligned trabeculae. In the third stage, there is proliferation and compaction of the outer layers and the invasion of the coronary vessels into the mantle of muscle fibers from the epicardial surface. In the fourth stage, the morphogenesis of transmural helical layers is complete with the coronary vascular tree as seen in the adult heart.

The helical arrangement of muscle fibers in the LV (Fig. 1D) is found across the evolution of various animal species. This natural occurring anatomical arrangement has fascinated anatomists over centuries (11–14). With the advent of modern histological techniques, studies have analyzed the architecture of the myocardium in transmural plugs of ventricular tissue that permitted a detailed examination within a given region of myocardium (15,16). These studies established that fiber orientation was a function of transmural location, with fiber direction being predominantly longitudinal in the endocardial region; transitioning into a circumferential direction in the midwall and becoming longitudinal again over the epicardial surface. Myofiber morphology was described either based on orientation of individual fibers or as multiple myocyte ‘sheet’ arrangements separated by extensive ‘sheet cleavage’ planes (17–20). Some investigators depicted the LV as a complex nested continuum where the myofibers entwined to form a mechanical and electrical syncytium (21,22). Whether the myofibers are aggregated within the LV as fascicles or transmural bundles remains an area of unresolved debate (22–24).

To understand the helical myofiber orientation of the subendocardial and subepicardial regions, consider the counterdirectional orientation of fingers on superimposed human hands. If an ascending strand of helix turns in the direction of right hand’s fingers, it’s a right-handed helix, if it turns in the direction of the left hand it is a left-handed helix (Fig. 1E). Note that handedness is a property of the helix, not of the perspective: you can turn a right-handed helix around and it is still right-handed and cannot be superimposed over the left-handed helix. Such handedness that excludes superimposition is referred to as chirality. Indeed, several studies in experimental mechanics and computational modeling have described the LV wall as a chiral structure where right-handed helical myofiber geometry in the subendocardial region transitions gradually into a left-handed geometry in the subepicardial region (Fig. 1E) (7,25–27).

Therefore, the long axis of myofibers when viewed from outside the LV rotates clockwise from the endocardium towards the epicardium, with reported net difference in myofiber angulation ranging from +60° to −60° (15). In the short axis views, the myofibers are clustered within layers (myofiber sheets) that are separated by cleft spaces (cleavage planes). These layers are not aligned parallel to one another; rather, the myofiber sheets diverge within the LV wall creating angulations with respect to the plane of the epicardial surface. Debate continues concerning the magnitude and variability of this angular alignment. A recent study in porcine hearts indicated that about three-fifths of the myocardial cells had their long axes diverge within the LV wall at angles between 7.5° and 37.5° in comparison to the epicardial surface (28).

Effect of Myocardial Anisotropy on Appearance of Cardiac Ultrasound Images

Tissue appearance in echocardiographic images is to a great extent influenced by constructive and destructive interferences of different backscattering waves, resulting in speckle patterns (29). These patterns can be used for motion analysis (speckle tracking) (30). The anisotropic

structure of the LV wall, with fiber directions changing from a right-handed helix in the subendocardium to a left-handed helix in the subepicardium (Fig. 2A), alters the propagation and backscatter of ultrasonic waves (31–33). Previous investigations have shown that the integrated backscatter in the LV wall varies approximately as a sinusoidal function of the angle of insonification at each transmural level (31,34). Greater backscatter resulting in a brighter image area is observed when fibers are interrogated by an ultrasound beam that is approximately perpendicular rather than parallel to the direction of the fibers. For example, in the apical four-chamber view of the interventricular septum and lateral wall, bright speckles in the mid wall represent the location of circumferential fibers that run perpendicular to the echocardiographic scan plane (Fig. 2B) (34). Conversely, in short axis views of the LV, bright speckles are seen in the anterior and posterior segments where myofiber sheets are perpendicular to the line of propagation of ultrasonic beam, while prominent attenuation occurs within the midwall of the septum and the lateral segments where the myofiber sheets are relatively parallel (31). A high resolution transducer placed directly over the epicardial surface of a beating heart is used to demonstrate this phenomenon (Supplementary video 1). A transmural anisotropy can also be identified within the regions of LV that produce bright speckles in the short axis views. For example, the arrangement of myofibers within the subendocardial and subepicardial layers of the bright anterior segment in the short axis view of the LV produce a distinctive counterdirectional movement of the orthogonally related fiber layers in a beating heart (Supplementary video 2).

Electrical Sequence

Depolarization

Electrical activation begins subendocardially in the right-handed helix near the apical septum and spreads rapidly toward the base (35). Recent investigations in humans have confirmed that the earliest epicardial electrical break-through occurs in the right ventricular free wall and the anterior LV wall, and then travels in an apex-to-base direction (36). The basal posterior wall is the last region to be activated, which occurs during the down-slope of the R-wave (36). The timing and sequence of electrical excitation in the ventricles is influenced by the impulse propagating through the His-Purkinje system and the anistropic nature of myocardium where propagation velocities are faster along rather than across the fibers (35,37). Higher velocities along the fiber direction are partially attributed to a high density of gap junctions (connection sites allowing the passage of ions from cell to cell) concentrated at the intercalated disks in the longitudinal direction (as compared to cross-fiber gap junction densities) (38). As a consequence, the electrical wavefront travels from the endocardium towards the epicardium in a clockwise rotation, along the orientation of the myofibers within the LV wall (37).

Repolarization

During repolarization, transmural electrical gradients propagate in a base-to-apex direction, which has been confirmed by recent experimental studies (39,40). The apical subepicardium is the last region to complete its repolarization, with regional bipolar signals persisting beyond the T-wave of the surface ECG (41). This period has been traditionally reserved for the identification of the U-wave on the surface ECG. Einthoven originally described this ECG deflection and attributed it to late repolarization of regional ventricular myocardium (42). Whether prolonged repolarization of the apical epicardium actually plays a role in the genesis of physiological U-waves requires further confirmation.

Mechanical Sequence: Experimental Observations

Sonomicrometry has been established as the reference method for direct measurement of the instantaneous distance between any two miniature ultrasound crystals implanted within skeletal, smooth, or cardiac muscle (43,44).

Contraction

On comparing the shortening sequence within subendocardial and epicardial regions with sonomicrometry crystals, a temporal sequence of deformation emerges within each helical layer that tracks the direction of fiber arrangement (27,41). The rapid apico-basal spread of electrical activation within the subendocardium initiates the contraction sequence. The onset of subendocardial shortening coincides hemodynamically with an early rapid build-up of intraventricular pressure during the isovolumic contraction period (Fig. 3A). Subepicardial deformation occurs later temporally coinciding with the onset of systolic ejection (Fig. 3B). The temporal lag between the onsets of subendocardial and subepicardial contraction activities correlates with the duration of isovolumic contraction.

During isovolumic contraction, there is subendocardial (right-handed helical) shortening and simultaneous subepicardial fiber stretching (27). The biphasic deformations satisfy isovolumic mechanics: shortening in one direction is accompanied with stretching in the other direction. Stretching of the subepicardial myofibers initiates an intrinsic length-sensing mechanism (stretch activation), which allows muscle to adjust the force of subsequent shortening during ejection (45). During ejection, the ventricular cavity dimension shortens in all directions due to contraction of both subendocardial and subepicardial directions. However, shortening strains in the apical segments exceed those in the basal segments, such that the wave of shortening moves in the axial direction from the apex toward the base (41,46,47).

Relaxation

Reversal of the shortening-lengthening relationship defines the physiological onset of relaxation. Relaxation begins in the apical subendocardium (the right-handed helix) just before the closure of the aortic valve and spreads from apex-to-base during the period of isovolumic relaxation (41). Relaxation in the subepicardium (the left-handed helix) begins after aortic valve closure and evolves in the opposite direction, beginning at the base and progressing apically during early diastolic filling (41). Note that systole myofibers in both helices shorten from apex-to-base, thus milking blood out of the ventricle, while during diastole the two helices relax in opposite directions (apex-to-base for subendocardium and base-to-apex for subepicardium). The differences in onset of relaxation result from postsystolic shortening in apical subepicardial and basal subendocardial regions. Consequently, such ‘physiological’ postsystolic shortening of the LV myocardium creates active apex-to-base and transmural gradients of relaxation that are believed to play an important role in active diastolic restoration of the LV and creation of forces required for diastolic suction (41). During early diastolic filling, pressure at the LV apex is lower than at the base, which results in base-to-apex suction of blood.

Sequence of the LV Rotation

Shortening and lengthening of the myocardial wall results in rotatory movements because of the intrinsic spiral geometry of the myofibers. During isovolumic contraction, predominant shortening of the subendocardial fibers and stretching of the subepicardial fibers result in a brief clockwise rotation of the apex (right-handed helix rotation directed along subendocardial fiber direction) (41,48,49) (Fig. 4A). During ejection, myofibers shorten across the entire transmural wall of the LV. However, the direction of rotation is governed by the subepicardial

fibers owing to their longer arm of movement (50) and their intrinsic contractile properties (51). Shortening of subepicardial fibers results in counterclockwise rotation of the LV apex and clockwise rotation of the LV base. The net result is twist or torsion that results in a wringing movement of the LV.

Kinetic energy during systole is spent not only in ejection but also in conversion to potential energy by means of twisting the subendocardial fibers. During isovolumic relaxation, the twisted subendocardial fibers behave like a compressed coil that springs open while releasing the potential energy stored in the deformed matrix. This recoil is appreciated as a clockwise rotation of the LV apex. Diastolic untwisting is facilitated by progressive base-to-apex relaxation of the subepicardium. The apical epicardial segment is the last region to complete relaxation, which helps maintaining both base-to-apex and transmural gradients of relaxation for active diastolic restoration of the LV cavity (41). Because the subepicardial fiber sheets angle outwards toward the surface, continued shortening of this layer, with simultaneous subendocardial relaxation, results in outward directed forces that pull open the LV apex as it untwists.

Mechanical Sequence: Observation by Echocardiography

Isovolumic periods

Tissue Doppler velocity images show transient biphasic waveforms during the isovolumic periods (52,53). Within the isovolumic contraction (IVC) period, fiber shortening initially occurs within the subendocardial fiber layers (27) with the peak coinciding with mitral valve closure. Because the ventricular volume does not change, subendocardial shortening is counterbalanced by stretching principally in the subepicardial fibers. The resulting nearly simultaneous shortening and lengthening vectors form a biphasic velocity tracing in TDI (27). This phenomenon also accounts for a brief spike seen in strain or displacement waveforms during transitions between the isovolumic and ejection phases. Non-uniform movement of the subendocardial and subepicardial layers can also be recorded in the radial direction (Fig. 5A and B). When the subendocardial layers show an inward movement toward the cavity, a transient outward movement is recorded from the subepicardial layers and vice versa. The subendocardial and the subepicardial layers thus show a complementary biphasic pattern of movement during IVC and IVR.

Ejection Period

During ejection, myocardial strain is higher in apical segments as compared to base. This finding has been observed with sonomicrometry (41,47), magnetic resonance imaging (54) and 2-D speckle tracking (55). Fig 6 shows longitudinal strain recorded from the lateral wall of the LV by 2-D speckle tracking. Note that shortening strains at the onset of ejection are higher in the apex and progressively decrease toward the base. This phenomenon may explain why during ejection, the mitral annulus is pulled toward the apex.

For analyzing the spread of mechanical activation sequence, the sequence of longitudinal shortening provides information about the apex-to-base propagation of mechanical activation in the intact heart (Supplementary video 3). It should be noted that the apical cap of the LV is devoid of any longitudinal fibers; therefore, the curved apical cap is not included for analyzing the longitudinal shortening sequence. The apical cap and basal segments show some stretching during the early part of ejection (note that the early stretch of the LV apical cap can be palpated as apical impulse).

For illustrating the relevance of the apex-to-base shortening gradient, consider the example of a patient with severe dilated cardiomyopathy with spherical remodeling (Supplementary video 4). Longitudinal shortening of the lateral wall is dysfunctional with systolic stretching of the

apical segment. The direction of LV apical twist is also reversed (Fig. 4B and Supplementary videos 5 and 6). Longitudinal shortening is, however, preserved in the basal segment. The reversal of apical twist (Fig. 4B) and the longitudinal shortening gradient is associated with systolic ascent of the mitral annulus (Fig. 7). Thus, despite shortening of the LV basal segment, the mitral annulus ascends. This example substantiates the importance of the apex-to-base longitudinal shortening gradient in the normal descent of the mitral annulus during systolic ejection.

Early and late diastole

Postsystolic shortening of the subendocardium near the base continues till the onset of early diastolic filling and can be quantified by 2-D speckle tracking. Untwisting of the apex occurs predominantly during IVR, however, some amount of untwisting continues further into the phase of early diastole. Expansion of the LV cavity in diastole occurs in three sequential stages. First expansion at the apex coincides with the onset of IVR, following which the LV base expands coinciding with the onset of early diastolic filling and is followed subsequently by late diastolic filling. This completes the cardiac cycle.

LV intracavitary flow sequence

Contrast echocardiography (56,57) can provide important information regarding the 2-dimensional features of LV intracavitary flow during the different phases of cardiac cycle (Fig. 8A and B) (58). Contrast bubbles can be tracked in time and space for visualization of flow vectors in 2-, 3- or higher-dimensional images (56,57,59).

Contraction

During the pre-ejection phase (Fig. 8B, 1), even before the mitral valve has closed, blood flow begins to accelerate towards the base, consistent with the apex-to-base direction of electromechanical activation. This stream of blood accentuates a wake vortex across the anterior edge of the closing anterior mitral leaflet. The rearrangement and redirection of blood flow during the preejection phase temporally coincides with the biphasic movement of the LV wall observed on tissue Doppler imaging. Contraction in one direction (right-handed helix) and stretching in the orthogonal direction (left-handed helix) assist to displacement of the intracavitary flow toward the LV outflow. Further propulsion of blood from the LV cavity results in ejection (Fig. 8B, 2).

Relaxation

During IVR, a rapid base-to-apex reversal of blood flow is seen (Fig. 8B, 3). Before the mitral valve opens, blood momentum is redirected toward the apex, which prepares the ventricle to receive blood most efficiently. This rapid reversal of isovolumic intracavitary pressure and flow explains the physiologic relevance of early endocardial relaxation and opening of the LV cavity near the apex and subsequent opening of the mitral valve. During both early diastole and late diastole (Fig. 8B, 4 and 5), a larger vortex is formed across the anterior mitral leaflet and a smaller posterior vortex across the posterior mitral leaflet (57,60).

Spiraling Blood Flow in Arteries

Spiraling is also seen in the conduit arteries. Flow from the aortic root, through the ascending aorta, and into the descending aorta forms a right-handed helix (61). These findings are consistent with swirling flows in nature, where an efficient transfer of energy occurs through the formation of a vortex, compared with propulsion of fluid along a straight jet (60). Distortion of blood flow spiraling is associated with carotid artery atheromatous disease and renal function deterioration (62,63).

Conclusion

Structural anisotropy and functional heterogeneity is a characteristic feature and a prerequisite for normal performance of the LV. The myofiber structure of the LV changes from a right-handed helix in the subendocardium to a left-handed helix in the subepicardium. Electrical activation and deformation propagate in apico-basal and endo-epicardial directions, synchronizing the counterdirectional layers into a single synergistically functioning system. Energy spent in systole is used not only for ejection but also for torquing the subendocardial fibers. In the subsequent stage of relaxation, the subendocardial fibers are released like a compressed coil that springs open while expanding outward, facilitated by postsystolic shortening of the apical subepicardial and the basal subendocardial regions. This relaxation activity produces a rapid decrease of LV intracavitary pressure during IVR and promotes active suction in early diastole. These experimental observations provide reasoning for the pattern of LV deformation and torsion that is observed on real-time 2-dimensional echocardiography in humans.

Supplementary Material

Refer to Web version on PubMed Central for supplementary material.

Acknowledgements

This work was supported by grant HL68573 and, in parts, HL68555 and HL70363 from the National Institutes of Health and Grant in Aid from the American Society of Echocardiography

References

1. Klar AJ. Fibonacci's flowers. Nature 2002;417:595. [PubMed: 12050641]
2. Wurman J, Straka JM, Rasmussen EN. Fine-Scale Doppler Radar Observations of Tornadoes. Science 1996;272:1774–7. [PubMed: 8662481]
3. Lin CC. Global spiral patterns in galaxies: complexity and simplicity. Ann N Y Acad Sci 1998;867:229–52. [PubMed: 12088042]
4. Andersen A, Bohr T, Stenum B, Rasmussen JJ, Lautrup B. Anatomy of a bathtub vortex. Phys Rev Lett 2003;91:104502. [PubMed: 14525483]
5. Holdrege, C. The Heart: A Pulsing and Perceptive Center. In: Holdrege, C., editor. The Dynamic Heart and Circulation. Fair Oaks, CA: AWSNA Publications; 2002. p. 8
6. Schauberger, V. The Energy Evolution: Harnessing Free Energy From Nature. 4. Gateway: Bath; 2000.
7. Vendelin M, Bovendeerd PH, Engelbrecht J, Arts T. Optimizing ventricular fibers: uniform strain or stress, but not ATP consumption, leads to high efficiency. Am J Physiol Heart Circ Physiol 2002;283:H1072–81. [PubMed: 12181137]
8. Helm PA, Younes L, Beg MF, Ennis DB, Leclercq C, Faris OP, et al. Evidence of structural remodeling in the dyssynchronous failing heart. Circ Res 2006;98:125–32. [PubMed: 16339482]
9. Ashihara T, Namba T, Yao T, Ozawa T, Kawase A, Ikeda T, et al. Vortex cordis as a mechanism of postshock activation: arrhythmia induction study using a bidomain model. J Cardiovasc Electrophysiol 2003;14:295–302. [PubMed: 12716113]
10. Sedmera D, Pexieder T, Vuillemin M, Thompson RP, Anderson RH. Developmental patterning of the myocardium. Anat Rec 2000;258:319–37. [PubMed: 10737851]
11. Mall F. On the muscular architecture of the ventricles of the human heart. Am J Anat 1911;11:211–266.
12. McCullum JB. On the muscular architecture and growth of the ventricles of the heart. Johns Hopkins Hosp Rep 1900:307–335.
13. Pettigrew, AB. Design in Nature. Volume II. II. London: Longmans, Green and Co; 1908.

14. Torrent-Guasp F, Ballester M, Buckberg GD, Carreras F, Flotats A, Carrio I, et al. Spatial orientation of the ventricular muscle band: physiologic contribution and surgical implications. J Thorac Cardiovasc Surg 2001;122:389–92. [PubMed: 11479518]
15. Streeter DD Jr, Spotnitz HM, Patel DP, Ross J Jr, Sonnenblick EH. Fiber orientation in the canine left ventricle during diastole and systole. Circ Res 1969;24:339–47. [PubMed: 5766515]
16. Greenbaum RA, Ho SY, Gibson DG, Becker AE, Anderson RH. Left ventricular fibre architecture in man. Br Heart J 1981;45:248–63. [PubMed: 7008815]
17. LeGrice IJ, Takayama Y, Covell JW. Transverse shear along myocardial cleavage planes provides a mechanism for normal systolic wall thickening. Circ Res 1995;77:182–93. [PubMed: 7788876]
18. Arts T, Costa KD, Covell JW, McCulloch AD. Relating myocardial laminar architecture to shear strain and muscle fiber orientation. Am J Physiol Heart Circ Physiol 2001;280:H2222–9. [PubMed: 11299225]
19. Takayama Y, Costa KD, Covell JW. Contribution of laminar myofiber architecture to load-dependent changes in mechanics of LV myocardium. Am J Physiol Heart Circ Physiol 2002;282:H1510–20. [PubMed: 11893589]
20. Ashikaga H, Criscione JC, Omens JH, Covell JW, Ingels NB Jr. Transmural left ventricular mechanics underlying torsional recoil during relaxation. Am J Physiol Heart Circ Physiol 2004;286:H640–7. [PubMed: 14551052]
21. Hunter PJ, Smaill BH. The analysis of cardiac function: a continuum approach. Prog Biophys Mol Biol 1988;52:101–64. [PubMed: 3076684]
22. Anderson RH, Ho SY, Redmann K, Sanchez-Quintana D, Lunkenheimer PP. The anatomical arrangement of the myocardial cells making up the ventricular mass. Eur J Cardiothorac Surg 2005;28:517–25. [PubMed: 16179192]
23. Sedmera D. Form follows function: developmental and physiological view on ventricular myocardial architecture. Eur J Cardiothorac Surg 2005;28:526–8. [PubMed: 16126399]
24. Criscione JC, Rodriguez F, Miller DC. The myocardial band: simplicity can be a weakness. Eur J Cardiothorac Surg 2005;28:363–4. [PubMed: 15939612]author reply 364–7
25. Nielsen PM, Le Grice IJ, Smaill BH, Hunter PJ. Mathematical model of geometry and fibrous structure of the heart. Am J Physiol 1991;260:H1365–78. [PubMed: 2012234]
26. Chen J, Liu W, Zhang H, Lacy L, Yang X, Song SK, et al. Regional ventricular wall thickening reflects changes in cardiac fiber and sheet structure during contraction: quantification with diffusion tensor MRI. Am J Physiol Heart Circ Physiol 2005;289:H1898–907. [PubMed: 16219812]
27. Sengupta PP, Khandheria BK, Korinek J, Wang J, Belohlavek M. Biphasic tissue Doppler waveforms during isovolumic phases are associated with asynchronous deformation of subendocardial and subepicardial layers. J Appl Physiol 2005;99:1104–11. [PubMed: 15905326]
28. Lunkenheimer PP, Redmann K, Kling N, Jiang X, Rothaus K, Cryer CW, et al. Three-dimensional architecture of the left ventricular myocardium. Anat Rec A Discov Mol Cell Evol Biol 2006;288:565–78. [PubMed: 16705738]
29. Yu W, Yan P, Sinusas AJ, Thiele K, Duncan JS. Towards pointwise motion tracking in echocardiographic image sequences - Comparing the reliability of different features for speckle tracking. Med Image Anal 2006;10:317–330. [PubMed: 16464631]
30. Korinek J, Wang J, Sengupta PP, Miyazaki C, Kjaergaard J, McMahon E, et al. Two-dimensional strain--a Doppler-independent ultrasound method for quantitation of regional deformation: validation in vitro and in vivo. J Am Soc Echocardiogr 2005;18:1247–53. [PubMed: 16376750]
31. Wickline SA, Verdonk ED, Miller JG. Three-dimensional characterization of human ventricular myofiber architecture by ultrasonic backscatter. J Clin Invest 1991;88:438–46. [PubMed: 1864957]
32. Recchia D, Miller JG, Wickline SA. Quantification of ultrasonic anisotropy in normal myocardium with lateral gain compensation of two-dimensional integrated backscatter images. Ultrasound Med Biol 1993;19:497–505. [PubMed: 8236591]
33. Holland MR, Finch-Johnston AE, Wallace KD, Handley SM, Wilkenshoff UM, Perez JE, et al. Effects of tissue anisotropy and contrast acoustic properties on myocardial scattering in contrast echocardiography. J Am Soc Echocardiogr 1999;12:564–73. [PubMed: 10398915]

34. Sosnovik DE, Baldwin SL, Lewis SH, Holland MR, Miller JG. Transmural variation of myocardial attenuation measured with a clinical imager. Ultrasound Med Biol 2001;27:1643–50. [PubMed: 11839409]
35. Scher AM. Studies of the electrical activity of the ventricles and the origin of the QRS complex. Acta Cardiol 1995;50:429–65. [PubMed: 8932565]
36. Ramanathan C, Jia P, Ghanem R, Ryu K, Rudy Y. Activation and repolarization of the normal human heart under complete physiological conditions. Proc Natl Acad Sci U S A 2006;103:6309–14. [PubMed: 16606830]
37. Punske BB, Taccardi B, Steadman B, Ershler PR, England A, Valencik ML, et al. Effect of fiber orientation on propagation: electrical mapping of genetically altered mouse hearts. J Electrocardiol 2005;38:40–4. [PubMed: 16226072]
38. Saffitz JE, Davis LM, Darrow BJ, Kanter HL, Laing JG, Beyer EC. The molecular basis of anisotropy: role of gap junctions. J Cardiovasc Electrophysiol 1995;6:498–510. [PubMed: 7551319]
39. Opthof T. In vivo dispersion in repolarization and arrhythmias in the human heart. Am J Physiol Heart Circ Physiol 2006;290:H77–8. [PubMed: 16373596]
40. Janse MJ, Sosunov EA, Coronel R, Opthof T, Anyukhovsky EP, de Bakker JM, et al. Repolarization gradients in the canine left ventricle before and after induction of short-term cardiac memory. Circulation 2005;112:1711–8. [PubMed: 16157774]
41. Sengupta PP, Khandheria BK, Korinek J, Wang J, Jahangir A, Seward JB, et al. Apex-to-Base Dispersion in Regional Timing of Left Ventricular Shortening and Lengthening. J Am Coll Cardiol 2006;47:163–72. [PubMed: 16386681]
42. Surawicz B. U wave: facts, hypotheses, misconceptions, and misnomers. J Cardiovasc Electrophysiol 1998;9:1117–28. [PubMed: 9817564]
43. Moon BR, Conley KE, Lindstedt SL, Urquhart MR. Minimal shortening in a high-frequency muscle. J Exp Biol 2003;206:1291–7. [PubMed: 12624164]
44. Derumeaux G, Ovize M, Loufoua J, Pontier G, Andre-Fouet X, Cribier A. Assessment of nonuniformity of transmural myocardial velocities by color-coded tissue Doppler imaging: characterization of normal, ischemic, and stunned myocardium. Circulation 2000;101:1390–5. [PubMed: 10736282]
45. Campbell KB, Chandra M. Functions of stretch activation in heart muscle. J Gen Physiol 2006;127:89–94. [PubMed: 16446501]
46. Prinzen FW, Augustijn CH, Allessie MA, Arts T, Delhaas T, Reneman RS. The time sequence of electrical and mechanical activation during spontaneous beating and ectopic stimulation. Eur Heart J 1992;13:535–43. [PubMed: 1600995]
47. Buckberg GD, Castella M, Gharib M, Saleh S. Active myocyte shortening during the ‘isovolumetric relaxation’ phase of diastole is responsible for ventricular suction; ‘systolic ventricular filling’. Eur J Cardiothorac Surg 2006;29(S1):S98–S106. [PubMed: 16567105]
48. Gibbons Kroeker CA, Ter Keurs HE, Knudtson ML, Tyberg JV, Beyar R. An optical device to measure the dynamics of apex rotation of the left ventricle. Am J Physiol 1993;265:H1444–9. [PubMed: 8238432]
49. Kroeker CA, Tyberg JV, Beyar R. Effects of ischemia on left ventricular apex rotation. An experimental study in anesthetized dogs. Circulation 1995;92:3539–48. [PubMed: 8521577]
50. Taber LA, Yang M, Podszus WW. Mechanics of ventricular torsion. J Biomech 1996;29:745–52. [PubMed: 9147971]
51. Davis JS, Hassanzadeh S, Winitsky S, Lin H, Satorius C, Vemuri R, et al. The overall pattern of cardiac contraction depends on a spatial gradient of myosin regulatory light chain phosphorylation. Cell 2001;107:631–41. [PubMed: 11733062]
52. Lind B, Nowak J, Cain P, Quintana M, Brodin LA. Left ventricular isovolumic velocity and duration variables calculated from colour-coded myocardial velocity images in normal individuals. Eur J Echocardiogr 2004;5:284–93. [PubMed: 15219543]
53. Lind B, Eriksson M, Roumina S, Nowak J, Brodin LA. Longitudinal isovolumic displacement of the left ventricular myocardium assessed by tissue velocity echocardiography in healthy individuals. J Am Soc Echocardiogr 2006;19:255–65. [PubMed: 16500487]

54. Bogaert J, Rademakers FE. Regional nonuniformity of normal adult human left ventricle. Am J Physiol Heart Circ Physiol 2001;280:H610–20. [PubMed: 11158958]

55. Sukmawan R, Watanabe N, Toyota E, Wada N, Okahash N, Kume T, et al. Application of Novel Echocardiographic Two-Dimensional Tracking System to Define Regional Heterogeneity of Radial and Longitudinal Myocardial Strain and Strain-Rate. Circulation 2005;112:2561.

56. Mukdadi OM, Kim HB, Hertzberg J, Shandas R. Numerical modeling of microbubble backscatter to optimize ultrasound particle image velocimetry imaging: initial studies. Ultrasonics 2004;42:1111–21. [PubMed: 15234173]

57. Sengupta PP, Khandheria BK, Korinek J, Jahangir A, Yoshifuku S, Milosevic I, et al. Time resolved sequence of left ventricular flow redirection during isovolumic intervals of the cardiac cycle. J Am Coll Cardiol 2006;47:110A–110A.

58. Sengupta PP, Khandheria BK, Korinek J, Jahangir A, Yoshifuku S, Milosevic I, et al. Left ventricular isovolumic flow sequence during sinus and paced rhythms: New insights from use of high-resolution Doppler and ultrasonic digital particle imaging velocimetry. J Am Coll Cardiol. 2006accepted

59. Zheng H, Mukdadi O, Hertzberg J, Shandas R. Advantages in using multi-frequency driving ultrasound for optimizing echo particle image velocimetry techniques. Biomed Sci Instrum 2004;40:371–6. [PubMed: 15133986]

60. Gharib M, Rambod E, Kheradvar A, Sahn DJ, Dabiri JO. Optimal vortex formation as an index of cardiac health. Proc Natl Acad Sci U S A 2006;103:6305–8. [PubMed: 16606852]

61. Frazin LJ, Lanza G, Vonesh M, Khasho F, Spitzzeri C, McGee S, et al. Functional chiral asymmetry in descending thoracic aorta. Circulation 1990;82:1985–94. [PubMed: 2242523]

62. Houston JG, Gandy SJ, Sheppard DG, Dick JB, Belch JJ, Stonebridge PA. Two-dimensional flow quantitative MRI of aortic arch blood flow patterns: Effect of age, sex, and presence of carotid atheromatous disease on prevalence of spiral blood flow. J Magn Reson Imaging 2003;18:169–74. [PubMed: 12884328]

63. Houston JG, Gandy SJ, Milne W, Dick JB, Belch JJ, Stonebridge PA. Spiral laminar flow in the abdominal aorta: a predictor of renal impairment deterioration in patients with renal artery stenosis? Nephrol Dial Transplant 2004;19:1786–91. [PubMed: 15161949]

64. Henson RE, Song SK, Pastorek JS, Ackerman JJ, Lorenz CH. Left ventricular torsion is equal in mice and humans. Am J Physiol Heart Circ Physiol 2000;278:H1117–23. [PubMed: 10749705]

65. Delhaas T, Kotte J, van der Toorn A, Snoep G, Prinzen FW, Arts T. Increase in left ventricular torsion-to-shortening ratio in children with valvular aortic stenosis. Magn Reson Med 2004;51:135–9. [PubMed: 14705053]

Glossary

Vortex

Vortex defines a mass of fluid with a whirling or circular motion which tends to form a cavity or vacuum in the center of the rotation. Locking of the vortex motion in solid states results in vortex structural configurations identified in solids, for example in high temperature superconductors. Thus a number of new vortex states (vortex liquids, vortex glasses and solids) have been identified, which have created a new research area referred to as vortex matter.

Anisotropic

A term used to describe a structure or a physical property which varies with the direction of measurement.

Chiral

In geometry, a figure is **chiral** (and said to have **chirality**) if the object (e.g., helix) cannot be superimposed on its mirror image regardless of how the particular helix is manipulated.

Strain

Strain is a dimensionless quantity representing a fractional or percentage change from the original dimension; in echocardiography, LV wall longitudinal lengthening and transmural thickening are denoted by a positive strain, whereas longitudinal shortening and transmural thinning are denoted by negative strains.

Strain Rate

Strain rate is strain per time unit, i.e. the temporal derivative of strain.

Speckle

The gray scale image is seen to consist of a speckled pattern. The pattern is not the actual image of the scatterers in the tissue itself, but the interference pattern generated by the reflected ultrasound. Each region of the myocardium has its own unique speckle pattern which remains stable from one frame to the other. This can be appreciated on M-mode imaging.

Rotation

Rotation refers to the rotation of short-axis sections of LV as viewed from the apical end and defined as the angle between radial lines connecting the center of mass of that specific cross sectional plain to a specific point in the myocardial wall at end diastole and at any other time during systole. The unit of rotation is degrees or radians.

Twist or Torsion

Left ventricular twist and torsion are terms used in literature for explaining the wringing motion of the LV. Twist defines the base to apex gradient in rotation angle along the longitudinal axis of the LV and is expressed in degrees/cm, or radians per meter (64). Torsion and twist are equivalent terms. Torsion can also be expressed as the axial gradient in rotation angle multiplied by the average of the outer radii in apical and basal cross-sectional planes, thereby representing the shear deformation angle on the epicardial surface (unit degrees or radians) (65). This normalization can be used as a method for comparing torsion for different sizes of LV.

Net twist angle

When the apex-to-base difference in LV rotation is not normalized, the absolute difference (also in degrees or radians) is stated as the net LV twist angle.

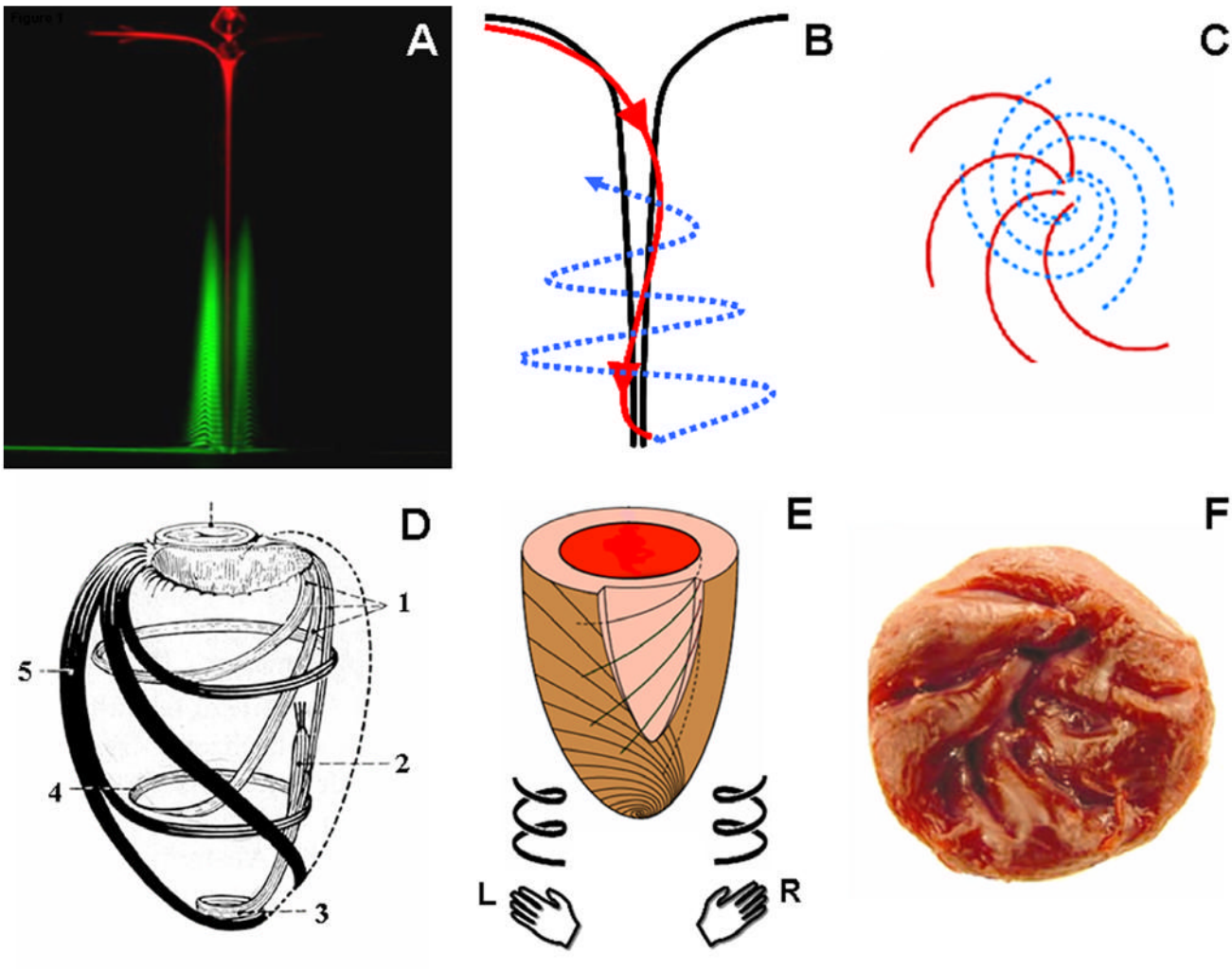

Figure 1.

Anatomy of a vortex. Two fluorescent dyes identify the counterdirectional swirls in a vortex: inner descending (red) and outer ascending (green) swirls (A, reproduced from (4) with permission). The longitudinal view (B) of the two counterdirectional swirls (red, descending; blue, ascending) is compared with the end on view from the surface of the vortex (C). There is a striking similarity between a vortex and the clockwise descending and counterclockwise ascending loops of myofibers in the LV (D, reproduced from (5) with permission). Fibers in the LV resemble a state of 'locked vortex'. The subendocardial region follows a geometric configuration of right-handed helix, while subepicardial fibers are in form of a left-handed helix (E). The right-handed helical arrangement of the subendocardial region can also be identified in the arrangement of trabeculae in the LV (F). L, left handed; R, right handed; 1, subendocardial fibers; 2, papillary muscle; 3, vortex cordis; 4, circumferential fibers; 5, subepicardial fibers

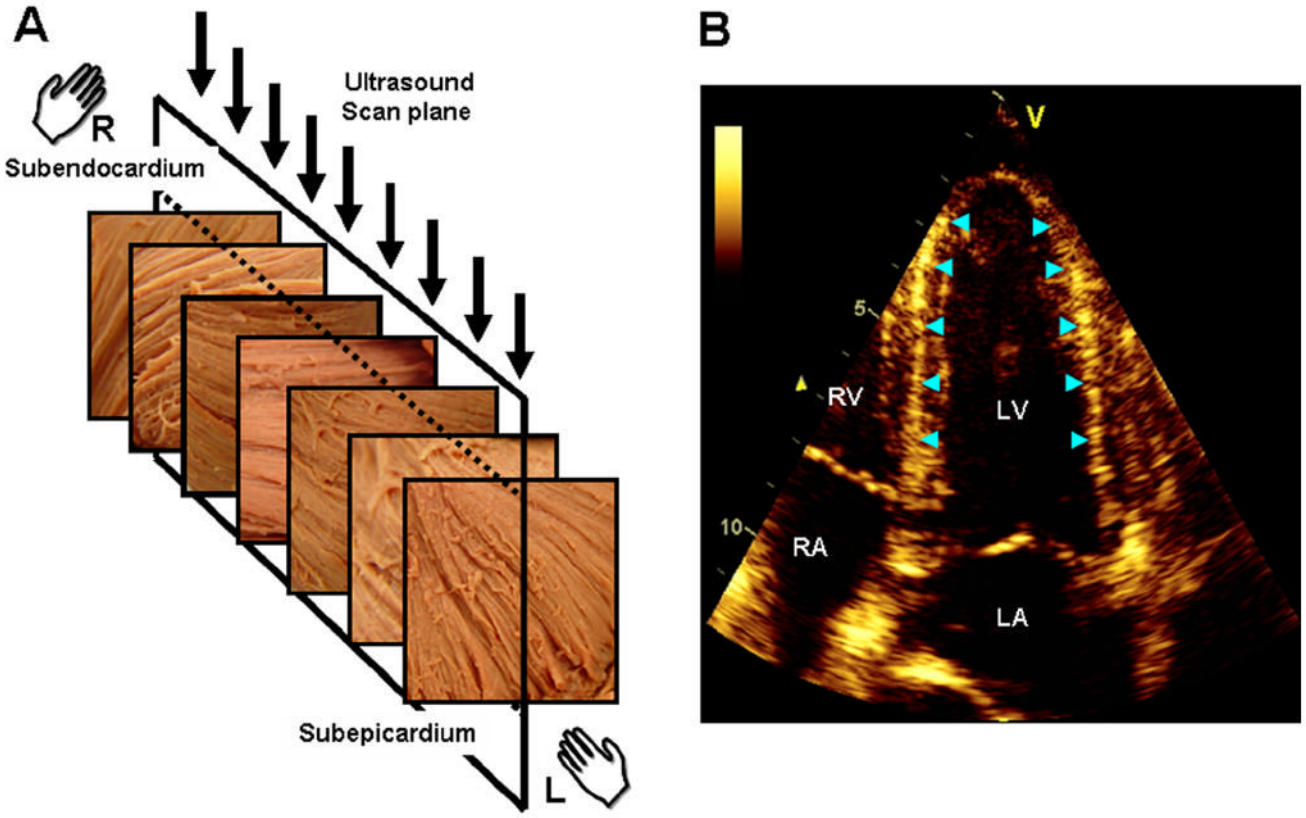

Figure 2.

Illustration of the link between the transmural variation of myocardial fiber direction (A) and the speckle pattern generated in echocardiography (B) (adapted from (34)). The fiber direction changes from a right-handed helix in the subendocardium to a left-handed helix in the subepicardium. The direction of myofibers is predominantly circumferential in the midwall. The ultrasonic image plane in apical 4-chamber view (A, arrows) is, therefore, orthogonal to the circumferentially oriented fibers in the midwall. The region of LV wall where fibers are orthogonal to the plane of ultrasound produce bright speckles and can be readily identified in the septum and lateral wall of the LV (B, arrow heads). LV, left ventricle; LA, left atrium; RV, right ventricle; RA, right atrium

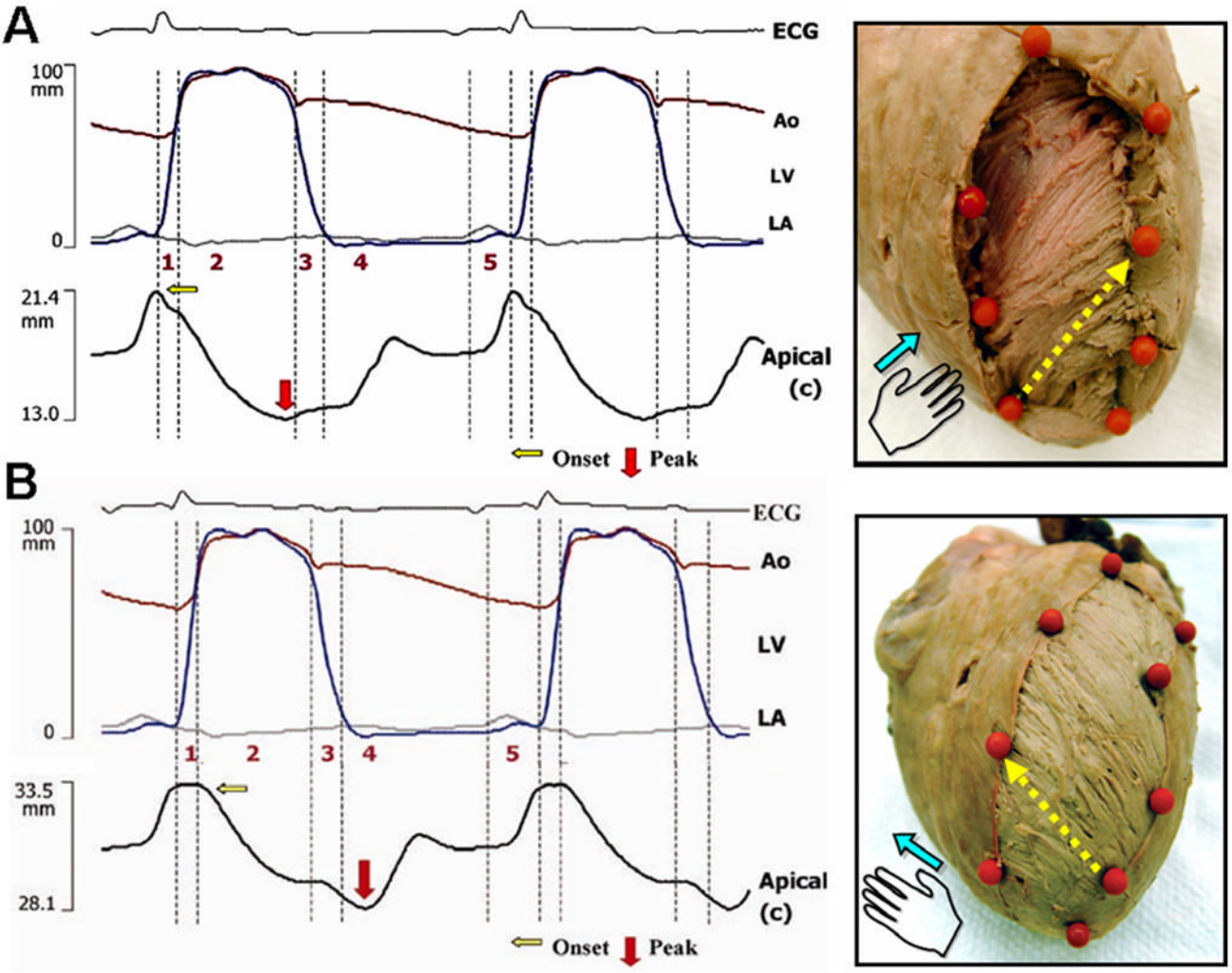

Figure 3.

Transmural sequence of deformation in the left ventricle using sonomicrometry. During isovolumic contraction, shortening is initiated along the subendocardial (right-handed helical) fiber direction (A). Onset of shortening in the subepicardial (left-handed helical) fiber direction is delayed and coincides with the onset of left ventricular ejection (B). The tissue specimens on the right show the corresponding subendocardial and subepicardial fiber arrangements, the position of sonomicrometry crystals (orange markers), and pairs of crystals used to determine deformation along the fiber direction (yellow arrows). Phase 1, preejection; 2, ejection; 3, isovolumic relaxation; 4, early diastole; 5, late diastole. Ao, aorta (red tracing); ECG, electrocardiogram; LA, left atrium (gray tracing); LV, left ventricle (blue tracing).

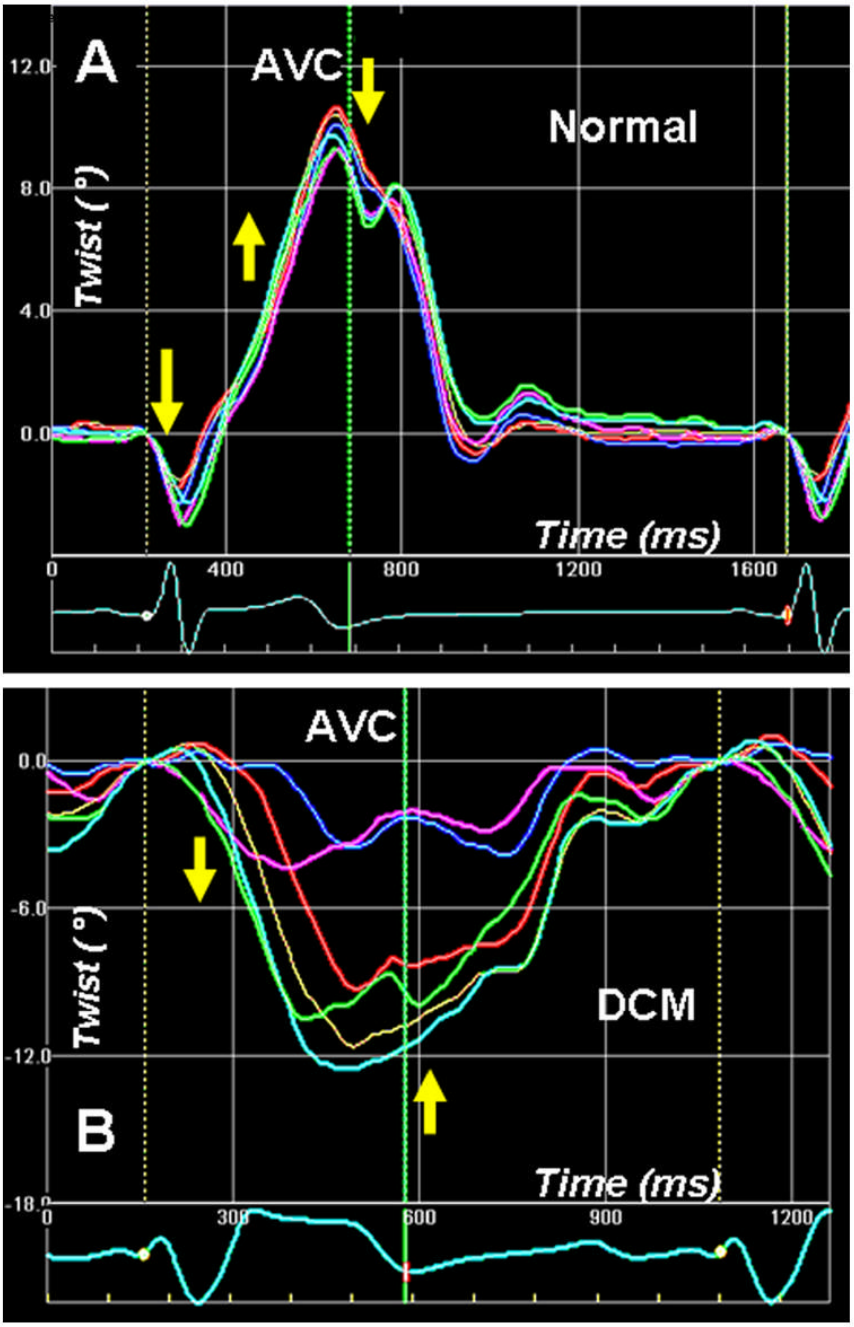

Figure 4.

Left ventricular apex rotation (twist) measured by 2-D speckle tracking of B-mode ultrasound images (2D strain) in a normal individual (A). An initial clockwise rotation occurs during the preejection period, followed by counterclockwise twisting during the ejection phase. Clockwise untwisting occurs predominantly during the phase of isovolumic relaxation. The adjoining panel (B) shows apical twist in a patient with dilated cardiomyopathy with dysfunctional apex. The apical twist sequence is completely the reverse of normal, i.e. apex rotates in clockwise direction during ejection, and in counterclockwise direction in diastole. Phases 1–5 are described in Fig. 3 legend.

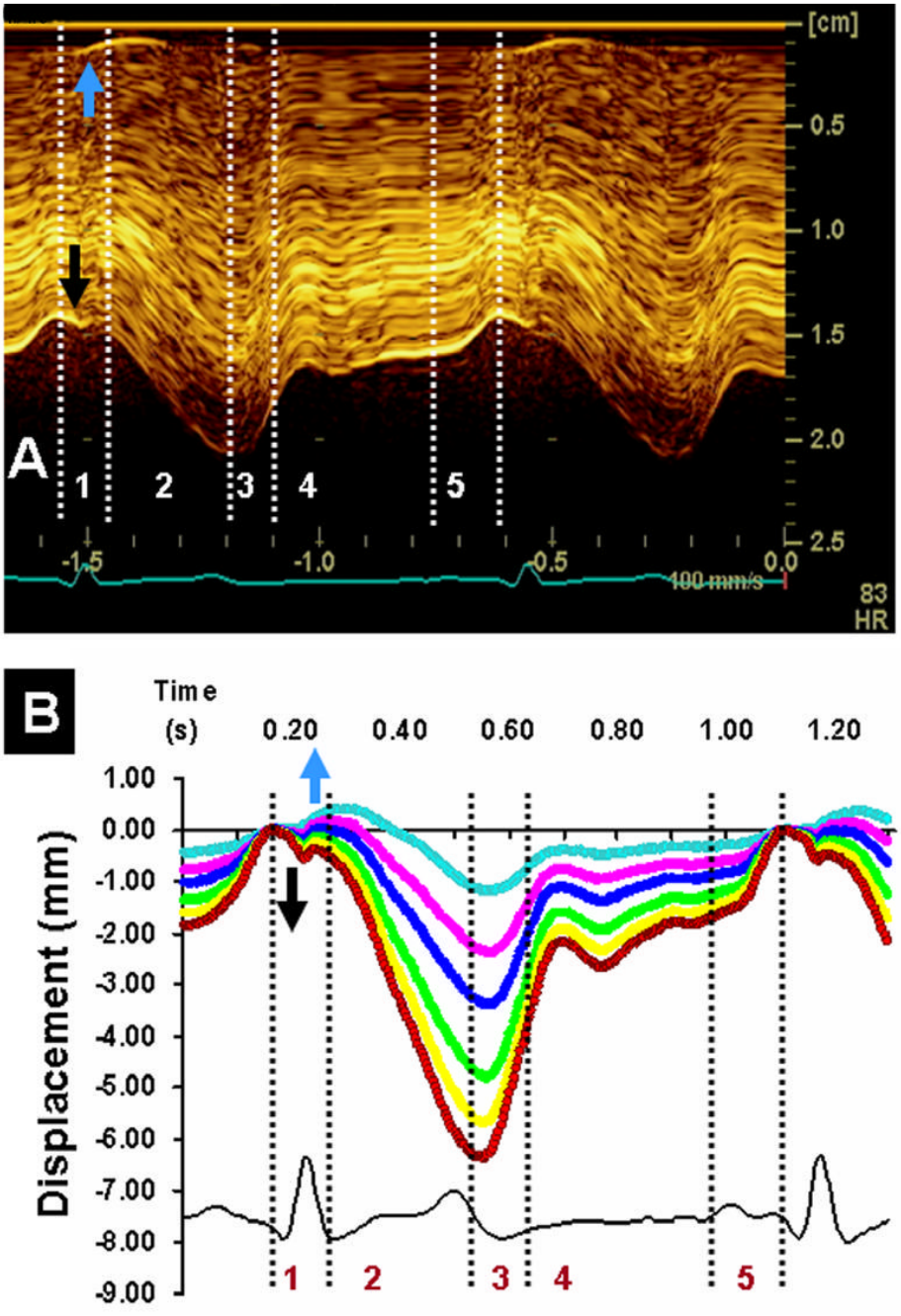

Figure 5.

Direct in vivo imaging of anterior wall of a beating porcine left ventricle using high-resolution linear array transducer (10 mHz). Panel **A** shows anatomic M-mode imaging of the different layers of anterior segment of left ventricular apex at high temporal resolution (250 frames/sec). During isovolumic contraction, there is onset of motion of the endocardium towards the cavity (black arrows) and a reciprocal outward motion of the subepicardium (blue arrows). These reciprocal movements of the subendocardial and subepicardial regions are distinct on tracking movement of speckles at different depths of myocardial wall (panel B). Displacement of the subendocardial region shows an inward movement (red), whereas the subepicardial region

shows an outward movement (blue) during the isovolumic period of the cardiac cycle. Phases 1–5 are described in Figure 3 legend.

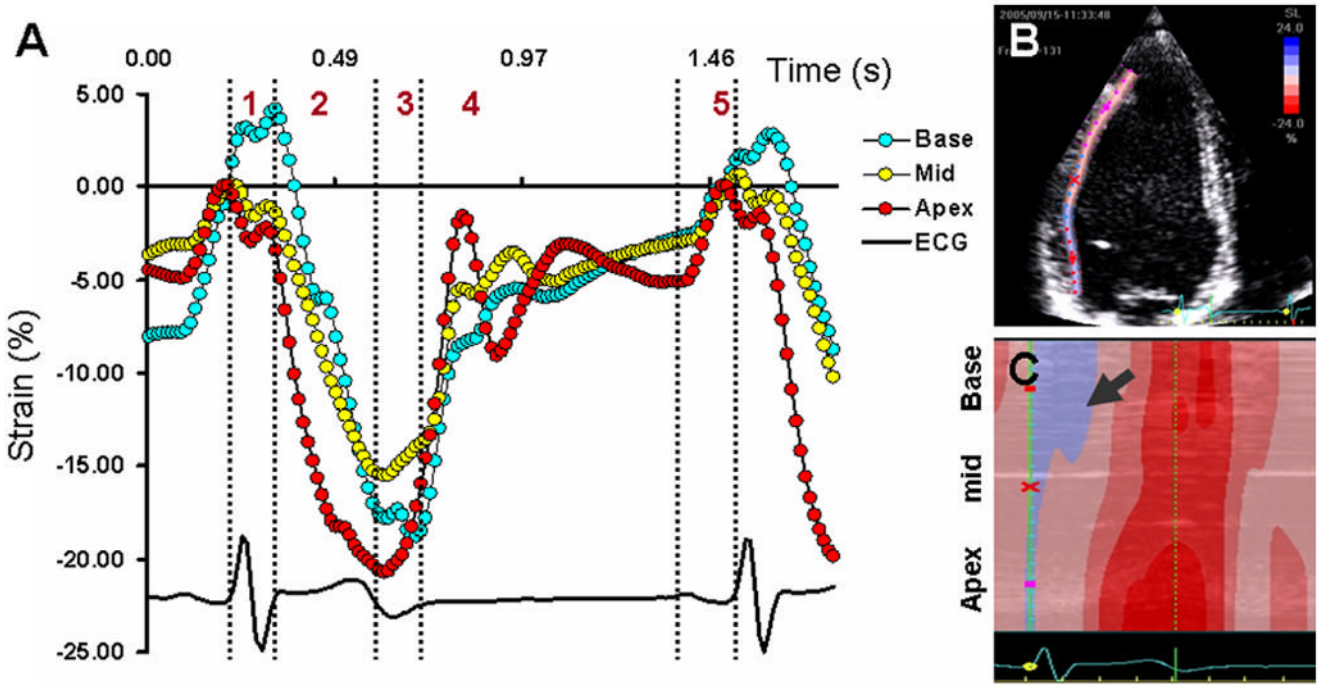

Figure 6.

Apex-to-base gradient of longitudinal deformation in the lateral wall of the left ventricle (LV) obtained by 2-D speckle tracking of B-mode ultrasound images (2-D strain) in a healthy adult female. Onset of longitudinal shortening occurs in the apical segment (panel A, red) and is delayed for the basal segment (Panel A, blue) of the LV. During ejection, shortening strains at the apex are higher than that at the base. Shortening-lengthening cross-over of the basal segment is delayed till the end of isovolumic relaxation Panel B shows the region of speckle tracking in lateral wall of the LV. Panel C shows the color M-mode profile of the longitudinal strains obtained from basal, mid and apical segments. Note the delayed onset of longitudinal shortening in the basal segment (arrow). The presence of blue color indicates presence of prestretching, while the apical and mid regions have already started shortening. Phases 1–5 in panel A are described in Figure 3 legend. ECG, electrocardiogram

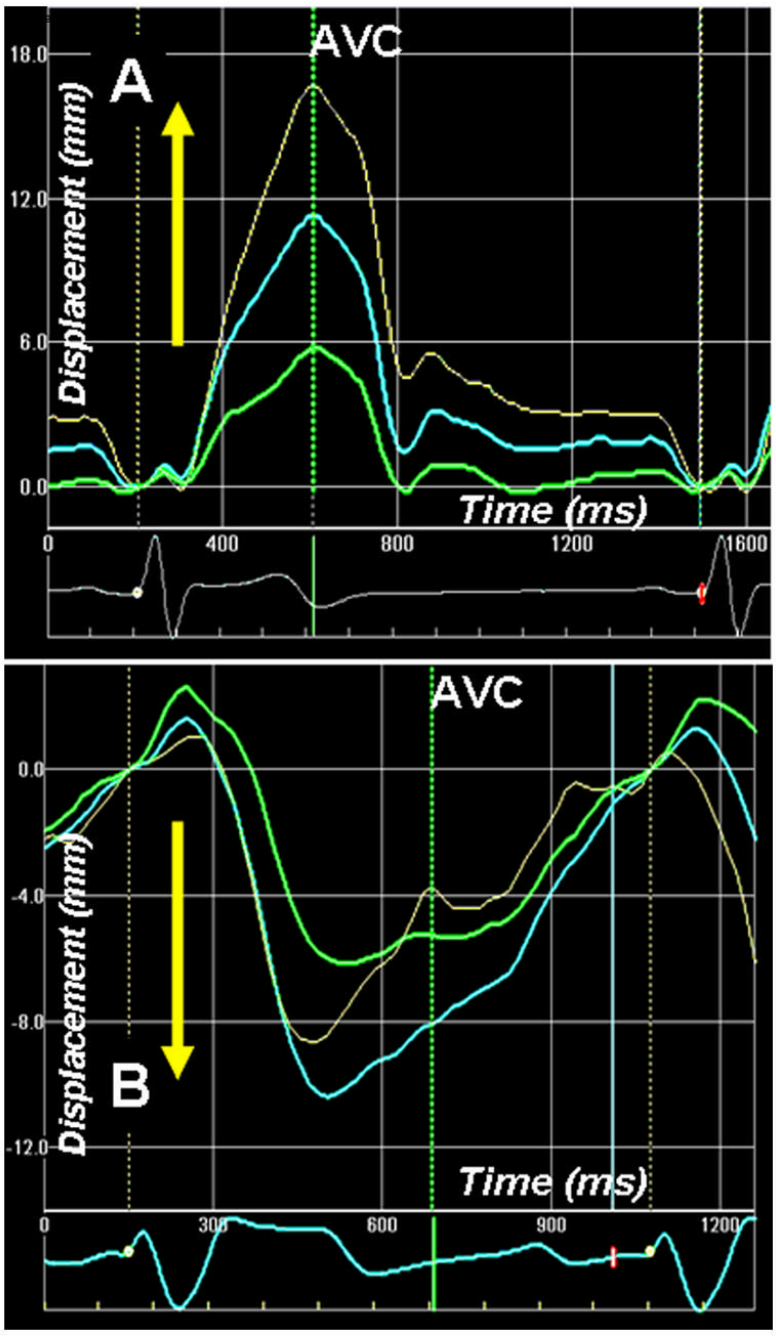

Figure 7.

Apex-to-base longitudinal displacement of the left ventricle (LV) measured by 2-D speckle tracking of B-mode ultrasound images (2 D strain) in normal (A) and a patient with dilated cardiomyopathy (also shown in Figure 4). In normal healthy individual, the LV base descends towards the apex and there is base-to-apex gradient of longitudinal displacement. Note that the descent of the LV base towards the apex is associated with higher longitudinal shortening strains from the LV apex (Figure 4). The longitudinal strain gradient is reversed in patient with dilated cardiomyopathy (figure 4). This is associated with paradoxical longitudinal ascent of the LV base in systole. Phases 1–5 are described in Fig. 6 legend.

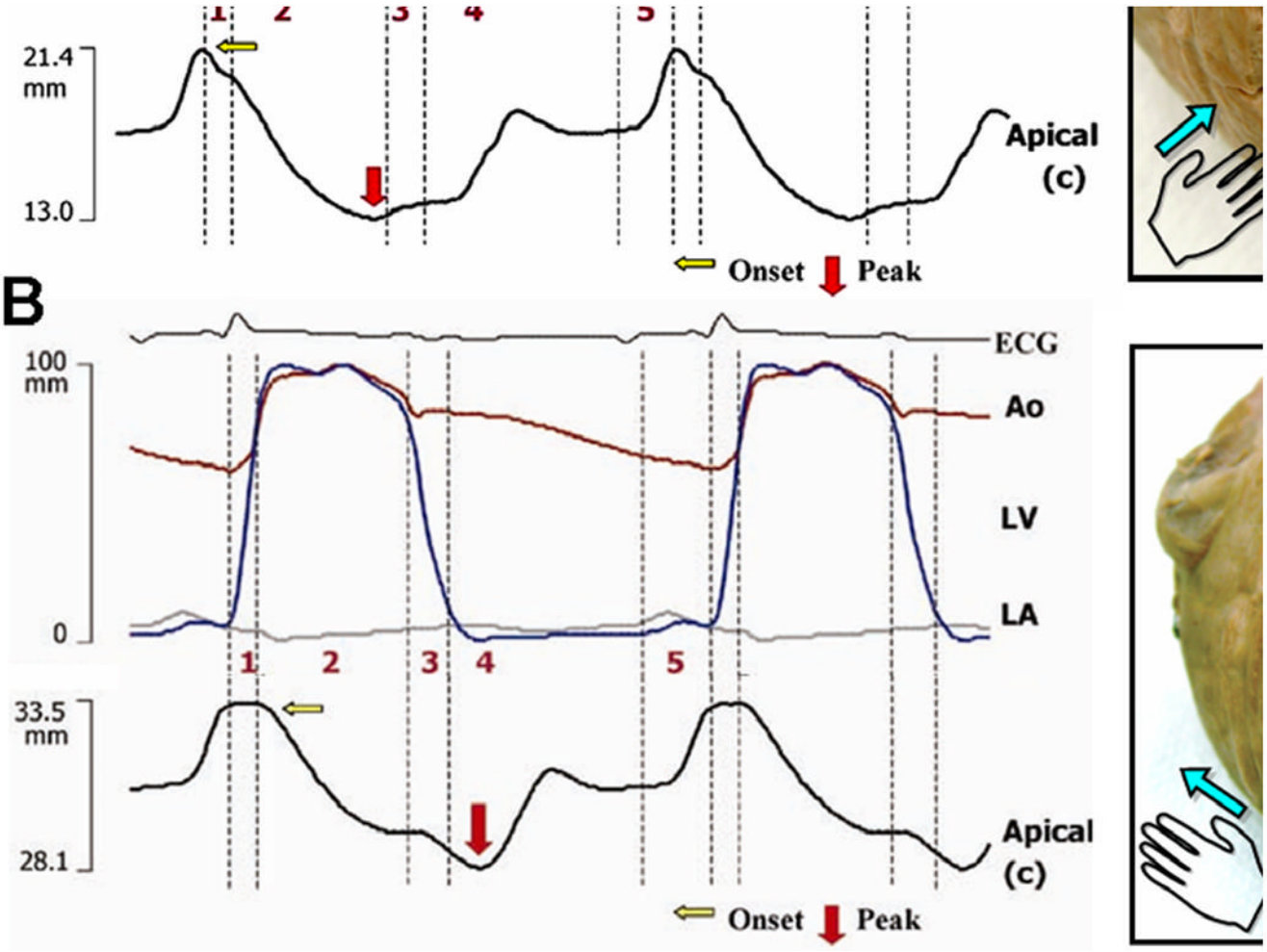

Figure 8.

Left ventricular flow during phases of cardiac cycle. M-mode characteristics of left ventricular intracavitary flow has been obtained with anatomical M-mode obtained along the long axis of the LV cavity during contrast infusion (A). Time-related changes in intracardiac flow in 2-dimension has been obtained by using high–temporal resolution 2D imaging at 200–250 frames/s and echo contrast particle imaging velocimetry (B). High frame rates allow tracking of bubbles sufficiently to determine the 2D component of local vectors of blood motion before the bubbles move out of the scan plane. For each phase, the local ensemble-averaged axis-normal velocity magnitude is superimposed on the vector field. **1**, Isovolumic contraction. **2**, Ejection. **3**, Isovolumic relaxation. **4**, Early diastole. **5**, Late diastole. LA, left atrium; LV, left ventricle